International Journal of Microwave and Wireless Technologies

cambridge.org/mrf

Dispersion properties of glide-symmetric corrugated metasurface waveguides

Boris Fischer[1,2] and Guido Valerio[1,2]

[1]Sorbonne Université, CNRS, Laboratoire de Génie Electrique et Electronique de Paris (GeePs), 75252, Paris, France and [2]Université Paris-Saclay, CentraleSupélec, CNRS, GeePs, 91192, Gif-sur-Yvette, France

Research Paper

Cite this article: Fischer B, Valerio G (2023). Dispersion properties of glide-symmetric corrugated metasurface waveguides. *International Journal of Microwave and Wireless Technologies* **16**(1), 13–20. https://doi.org/10.1017/S1759078723000090

Received: 10 December 2022
Revised: 3 February 2023
Accepted: 4 February 2023

Keywords:
corrugated parallel-plate waveguide; metasurfaces; analytic methods; mode matching; glide symmetry; broadband

Abstract

In this paper, a mode-matching procedure is used to prove for the first time the dispersionless behavior of glide symmetry (GS) in corrugated metasurface waveguides. Depending on their field symmetry, the Floquet harmonics have a different impact onto the frequency dispersion, which is reduced with GS when the gap between the surfaces is small. Indeed, the glide-symmetric waveguide is shown to have the same effective propagation features as a scaled mirror-symmetric waveguide with half the period and a doubled gap. We propose closed-form formulas for the effective refractive index of the glide-symmetric waveguide in the first Brillouin zone, having a small groove compared to the period. The closed-form expressions analytically prove the dispersionless behavior of GS.

Introduction

The increasing need of millimeter-wave communications in modern wireless communication systems [1] makes metasurfaces a promising technology capable of avoiding expensive and lossy electronic beam-forming systems [2, 3]. However, to be employed in practical devices, their propagation characteristics must be stable over a large bandwidth. Indeed, despite simple control of the propagation characteristics with the cell geometry, artificial materials tend to be dispersive i.e., their propagation characteristics change with frequency [4]. Therefore, one seeks for metamaterials with low dispersion [5].

In recent years, low-dispersive behavior has been observed for metamaterials displaying special symmetries, called higher symmetries [6, 7]. The idea is that the periodicity of the cells is broken from one cell to the next by introducing an additional geometrical operation e.g., rotation (twist symmetry) or translation (glide symmetry, GS). It is observed that metamaterials with such higher symmetries have less dispersion than their non-symmetric counterparts [8–10] and can achieve high degrees of anisotropy over large bandwidths, allowing for transformation optics of flat lenses [11]. Moreover, this low-dispersive behavior seems to be associated to the lack of certain stopbands that naturally occur for periodic metasurfaces: the first stopband disappears, while the second stopband at higher frequencies becomes larger [12]. Not only does this increase the available propagation spectrum of these structures, but it also makes them candidates for low-loss guiding or filtering devices [9, 13–15] that allow for energy-efficient, low-cost and small-sized communication systems, and for artificial dielectrics used in 3-D lenses [16].

In this paper we aim at better understanding the physical effects of GS onto the dispersive behavior, and obtaining accurate closed-form results for the effective refractive index of a corrugated parallel-plate waveguide (PPW), in which GS is added (see Fig. 1). This kind of waveguide is considered here because it is sufficiently simple to obtain closed-form results and yet it illustrates the main physical properties of glide-symmetric (G-S) metasurfaces. Unfortunately, the design of these devices requires fast and reliable dispersive analyses for optimization purposes. These are made difficult due to the presence of small geometrical details in the geometry of the unit cell, and the very close proximity between the surfaces. Closed-form solutions of these kind of dispersive problems are rare [17], and yet would be beneficial for a fast design and physical insight. It is important to remark that well-known homogenization results of corrugated structures [18, 19] do not hold in the G-S configuration. If each metasurface could be homogenized separately, their mutual shift would not matter [20], while the dispersive behavior of the waveguide is affected by the presence of GS as long as the interaction between the surfaces is strong enough.

In Section 'Mode-matching formulation' we will briefly describe the mode-matching (MM) formulation used to compute the fields inside the waveguide, previously used in [21, 22]. In Section 'Dominant harmonics with glide symmetry', this formulation enables the study of the impact of the different field components onto the dispersive behavior of the waveguide, with or without GS. From this, and for a small gap between the metasurfaces, Section 'Same-dispersive scaled non-glide structure' establishes a dispersive equivalency between the

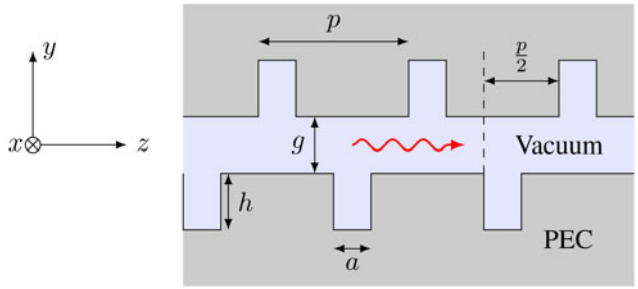

Fig. 1. All-metallic glide-symmetric corrugated metasurface waveguide. The structure is invariant along the x axis (corrugations direction), and is repeated periodically along the z-axis, which is the propagation direction of the waves. GS is introduced through the $p/2$-shift of the upper metasurface.

G-S waveguide and a scaled non-glide-symmetric (nGS) waveguide with half the period. These results are then used in Section 'Linearization of the low-dispersive curves' to obtain homogenized expressions for the refractive index seen by the first mode of the waveguide. Contrarily to the results derived in [23] in the quasi-static regime, the involved approximations are valid in the entire first Brillouin zone, which yields analytical proof of the low-dispersive behavior of GS. Unfortunately, these formulas are conditioned by geometrical restrictions on the corrugations. In Section 'Numerical results', we validate the closed-form expressions with numerical results.

An earlier version of this paper was presented at the XXI Mediterranean Microwave Symposium and was published in its Proceedings [24].

Mode-matching formulation

The fields are described in the Cartesian coordinate system $(x,\ y,\ z)$. The metallic corrugated metasurfaces are parallel to the xz-plane. Metallic losses are assumed to be negligible, that is the metasurfaces are perfectly electrically conducting (PEC). Wave propagation in the z-direction is studied, perpendicular to corrugations of depth h and width a. The origin of the coordinate system is located in between the two plates and right above the beginning of a corrugation, such that the lower plate is located at $y=-g/2$ and that there is a corrugation in the lower plate in the interval $0<z<a$. The corrugations are repeated periodically in the direction z with period p. If the corrugations of the upper plate are mirrored with respect to the propagation plane, the waveguide is nGS, whereas if there is an upper corrugation in the interval $p/2<z<p/2+a$, then the waveguide is G-S. Given that the structure is invariant along the x-direction, the structure can be studied in the yz-plane, as illustrated in Fig. 1. A MM analysis requires to express the fields in each region (the lower grooves, the gap between the surfaces, and the upper grooves) as a suitable sum of modes. Here, we will refer to the formulation proposed in [25].

The gap extends across the entire unit cell along the z-direction, so that the fields there can be written as a sum of Floquet harmonics. Each harmonic is characterized by its integer order s, which relates its propagation constant $\beta^{(s)}$ to the fundamental effective propagation constant β through the relation

$$\beta^{(s)}=\beta+s\frac{2\pi}{p}. \tag{1}$$

Floquet harmonics with an even order s have an antisymmetric longitudinal electric field with respect to the plane $y=0$. On the contrary, odd-order harmonics have a symmetric longitudinal electric field.

The grooves can be regarded as PPWs supporting propagation along the y-direction, shorted at their end, that is at $y=-\frac{g}{2}-h$. In each one of the lower grooves, the general form of the fields is a sum of parallel-plate transverse magnetic (TM) modes propagating in the y direction [4, pp.104–108]. Each mode is defined by its cut-off wavenumber $k_{y,m}=\sqrt{k_0^2-(\frac{m\pi}{a})^2}$, with k_0 the free-space wavenumber, and is weighted with coefficients c_m, $m\in\mathbb{N}$ being the index of the mode. In the upper grooves similar expressions can be written, but they are not necessary. By virtue of the GS, the generalized Floquet theorem bounds the fields of the upper corrugations to the fields in the lower corrugations [26–28]. The detailed field expressions on the lower corrugation surface can be found in [25] and are not repeated here.

The field continuity is then enforced across the junction between one lower groove and the gap. Enforcing GS takes into account the presence of the upper metasurface correctly shifted of half a period. Finally, a linear system is obtained

$$\underline{\boldsymbol{M}}\cdot\boldsymbol{c}=\boldsymbol{0}, \tag{2}$$

where the unknown vector $\boldsymbol{c}$ contains the grooves modal coefficients c_m. The entries of the square matrix $\underline{\boldsymbol{M}}$ contain the projections of groove modes on the Floquet harmonics in the gap. Each matrix coefficient relates two modes of orders m' and m, such that

$$M_{m'm}=\delta_{m'm}\frac{pa}{2^{\min\{1,m\}}}\frac{\cot(k_{y,m}h)}{k_{y,m}}-\sum_{s=-\infty}^{+\infty}f^{(s)}\frac{(-1)^{m'}4\beta^{(s)2}P_{m'}^{(s)}P_m^{(s)}}{k_y^{(s)}\left[\beta^{(s)2}-\left(\frac{m\pi}{a}\right)^2\right]\left[\beta^{(s)2}-\left(\frac{m'\pi}{a}\right)^2\right]}, \tag{3}$$

with the Krœnecker symbol $\delta_{m'm}$, and where $k_y^{(s)}=\sqrt{k_0^2-\beta^{(s)2}}$. Additionally, the term $P_m^{(s)}$ depends on the parity of the groove modes, that is

$$P_m^{(s)}=\begin{cases}\sin\left(\beta^{(s)}\frac{g}{2}\right), & \text{if } m \text{ is even},\\ \mathrm{j}\cos\left(\beta^{(s)}\frac{g}{2}\right), & \text{if } m \text{ is odd}.\end{cases} \tag{4}$$

The vertical field distribution of each Floquet harmonic in the gap results in the vertical spectral function

$$f^{(s)}=\begin{cases}-\cot\left(k_y^{(s)}\frac{g}{2}\right) & \text{if GS},\\ & \text{or if GS and } s \text{ is even},\\ \tan\left(k_y^{(s)}\frac{g}{2}\right) & \text{if GS and } s \text{ is odd}.\end{cases} \tag{5}$$

Ranging over the frequency f, or equivalently over k_0, the function $\beta(k_0)$ that allows for a non-zero solution $\boldsymbol{c}$ of (2) yields the effective propagation constant β of the fundamental Floquet mode supported by the waveguide. This function $\beta(k_0)$ is found

https://doi.org/10.1017/S1759078723000090

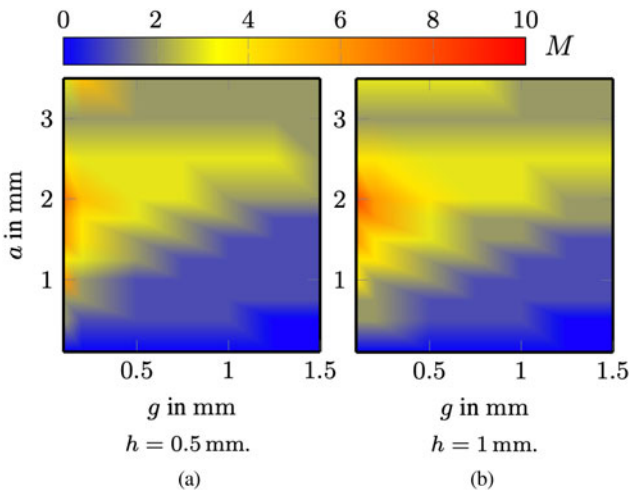

Fig. 2. Colormap of the number of corrugations modes $M+1$ required for the convergence of the G-S dispersion curve for $\beta < \pi/p$, depending on the gap g and the corrugation width a. 37 frequency points are computed for each curve, which is considered to converge when there is less than a 1% variation in β for all observation points. The cell width is $p = 4$ mm.

as the solution to

$$\det\left(\underline{\boldsymbol{M}}\right) = 0, \tag{6}$$

which is the dispersion equation of the G-S structure.

In a numerical framework, the infinite sums of harmonics and modes would need to be truncated, so that the matrix $\underline{\boldsymbol{M}}$ is of finite size in (6), that is $(M+1)\times(M+1)$ if M is the maximum order of the TM modes retained in the corrugations for the computation. In Fig. 2, the maximum mode order M needed to obtain acceptable convergence of the MM method in the first Brillouin zone in given as a function of the corrugation width a and the gap g, for G-S waveguides of period $p = 4$ mm and different corrugation depths h. A sufficiently large number of Floquet harmonics is considered as well. Fig. 2 illustrates how closely-lying metasurfaces cause strong multi-modal coupling, as indicated by the increasing M with small gaps g. Moreover, it appears that the coupling is strongest for medium-sized corrugations. Indeed, when $a = p/2$ in the G-S configuration, the edges of upper and lower corrugations are aligned, leading to maximal perturbation of the fields.

Dominant harmonics with glide symmetry

For the G-S structure, (3) seems to indicate that both even- and odd-order harmonics have an impact on the dispersive behavior of the waveguide. However, it can be shown that even-order harmonics are dominant when the gap g between the metasurfaces is small enough [29].

In (3), the wavenumber $k_y^{(s)}$ is imaginary, and so the vertical spectral functions (5) can rewritten as hyperbolic functions of a real variable. The hyperbolic cotangent function is strictly larger than the hyperbolic tangent. But this is not enough to state that the contributions of odd-order harmonics can be dismissed, as both hyperbolic tangent and cotangent converge to one for higher-order harmonics. Let $S > 0$ be the highest harmonic order to be considered in the truncation. In the first Brillouin zone (that is for $k_0 < \beta < \pi/p$) and for $1 < s \leq S$, harmonic wavenumbers defined in (1) are approximately frequency-independent, that is $\beta^{(s)} \simeq s2\pi/p$. Consequently, for the highest order S,

$$\frac{\coth\left(g2\sqrt{\left(\beta^{(S)}\right)^2 - k_0^2}\right)}{\tanh\left(g2\sqrt{\left(\beta^{(S)}\right)^2 - k_0^2}\right)} \simeq \frac{1}{\tanh^2\left(S\pi\frac{g}{p}\right)}. \tag{7}$$

If this ratio is large for the harmonic S, then this is the case for lower-order harmonics too, thus proving that all odd-order harmonics are negligible with respect to the even-order harmonics. For that to be true, $S\pi\frac{g}{p}$ must be small enough, yielding the condition

$$\left(S\pi\frac{g}{p}\right)^2 \ll 1. \tag{8}$$

Unfortunately, the number of harmonics S needed to obtain accurate dispersion curves can only be obtained by simulation, when the results converge. Indeed, due to the strong coupling between the G-S metasurfaces, S is itself a function of the waveguide parameters p, g, a and h. Yet, S can be estimated in the case where the required number of corrugation modes is known, e.g. through the data in Fig. 2. Indeed, [25] establishes that the ratio between the number of modes and harmonics must be equal to a/p in order for the field variations to be matched at the surface of the corrugations. If only two corrugation modes are needed, which seems to be the case for most gaps with $a = 1$ mm in Fig. 2, then around 9 harmonics are needed, that is $S = 4$. Nevertheless, it should also be noted that in all cases, the low-order harmonics have a larger impact on dispersion than high-order harmonics, that is the harmonics of orders 0 and ±1. A condition for the dominance of the fundamental harmonic over odd-order higher harmonics is then simply

$$g \ll \frac{p}{\pi}. \tag{9}$$

Therefore, when g is already smaller than a fraction of p/π, it is safe to state that the dispersive behavior of the waveguide is mainly influenced by the fundamental harmonic in the G-S configuration.

This is illustrated in Fig. 3a, where the Brillouin diagram of a G-S waveguide is plotted up to the first stopband. The CST results are compared to the convergent MM curves, with all harmonics or only the even-order harmonics. For small gaps, the even-order harmonics accurately describe the dispersive behavior, particularly for the first mode. On the other hand, for a nGS waveguide, all the harmonic terms in (3) are proportional to the cotangent independently of the order parity, as indicated by (5). Therefore, the odd-order harmonics cannot be dismissed from the dispersion equation, even for a small gap. That is why in Fig. 3b, keeping only the even-order harmonics yields inaccurate dispersion curves in the first Brillouin zone. Therefore, the derivation of (9) indicates how a small gap g leads the G-S waveguide to behave differently from its nGS counterpart. In this case, twice as many harmonics have dispersive impact in the nGS structure compared to the G-S structure. This leads to different harmonic couplings in both structures, and ultimately to a lower-dispersive behavior with GS. This is proven analytically in the next sections.

https://doi.org/10.1017/S1759078723000090

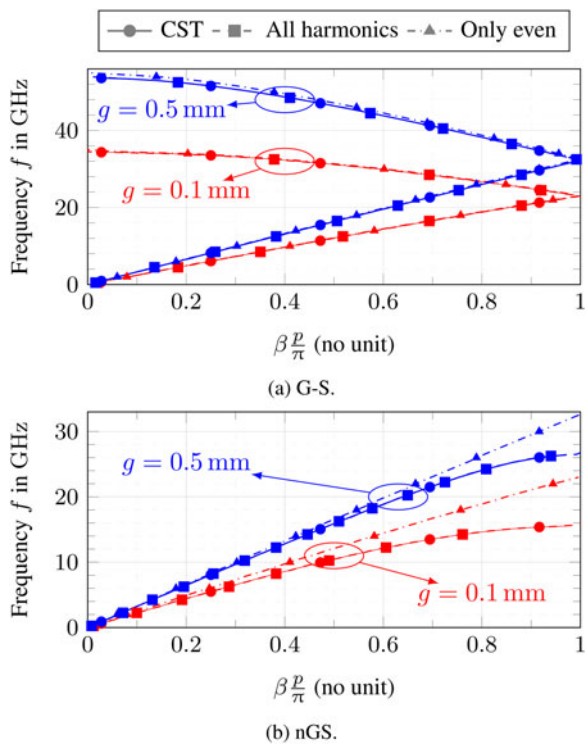

Fig. 3. Brillouin diagram of G-S and nGS corrugated PPWs with different gaps g between the metasurfaces. The CST results are compared to the MM method, either with all harmonics or only the even-order harmonics in the computation. All structures have $p = 4$ mm, $h = 0.5$ mm and $a = 1$ mm, (a) G-S, (b) nGS.

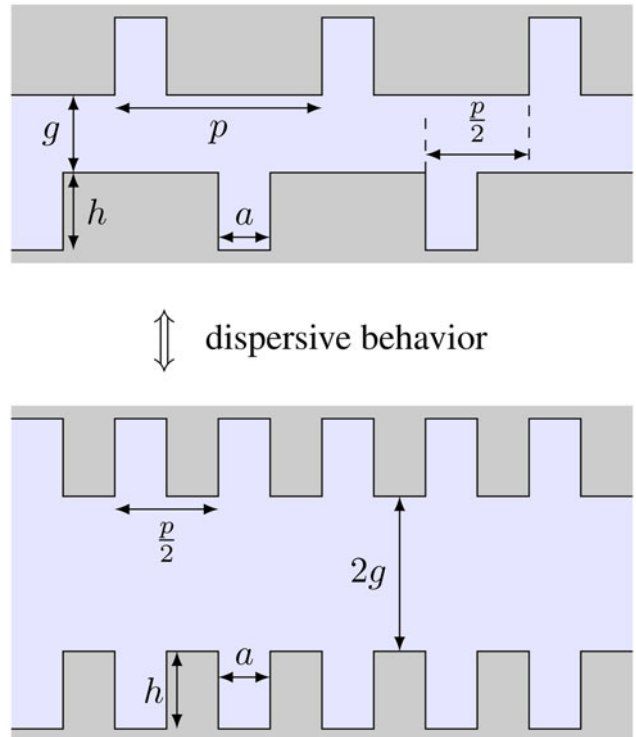

Fig. 4. Equivalent G-S corrugated PPW and nGS corrugated PPW with period $p/2$. This dispersive equivalence is true in the first Brillouin zone under the condition (8).

Same-dispersive scaled non-glide structure

In this section, we show that for a G-S corrugated PPW with a small gap, there exists a theoretical nGS structure that has the same dispersive properties. This equivalent structure gives insight about the linearity of the G-S dispersion curve.

If the gap g is small enough – satisfying condition (8)– then the symmetric harmonics of the G-S structure can be discarded. As such, the dispersion matrices of the G-S and the nGS structure are almost identical. The only difference is that the nGS structure has all harmonics, whereas the G-S structure only has harmonics with even order s. From this observation, it can be shown that the G-S corrugated PPW is equivalent to a scaled nGS structure in the first Brillouin zone. The periodicity $\hat{p}$ of this equivalent nGS structure must be half that of the G-S structure i.e., $\hat{p} = p/2$. Then, all the nGS harmonics with wavenumbers $\hat{\beta}^{(s)}$ can be identified to one of the even-order harmonics of the GS structure, given that

$$\hat{\beta}^{(s)} = \beta + s\frac{2\pi}{\hat{p}} = \beta + s\frac{4\pi}{p} = \beta + (2s)\frac{2\pi}{p} = \beta^{(2s)}. \tag{10}$$

Moreover, this equivalent nGS structure has a double gap $\hat{g} = 2g$. Then, it comes that for any dispersion matrix coefficient,

$$\hat{M}_{m'm} = \frac{1}{2}M_{m'm}, \tag{11}$$

where $\underline{\hat{\boldsymbol{M}}}$ is the dispersion matrix of the equivalent nGS waveguide. The 1/2-factor can be factored out of the matrix determinant, and so both structures have the same dispersion equation (6).

As such, the G-S and nGS structures sketched in Fig. 4 are equivalent in terms of dispersive behavior. Note that the equivalence is limited to the dispersive behavior, and that fields in these structures are not the same.

This equivalence may seem intuitive for a small corrugation width a. Indeed, in the G-S structure, every corrugation is faced with a PEC plate on the other side of the gap. If this PEC plate was infinite, it could be replaced by a symmetric corrugation at twice the gap, because of image theory [4, p. 44]. Nevertheless, this equivalence is intriguing for $a > p/2$. In this case, the equivalent nGS structure does not physically exist: the corrugation width a is larger than the cell-length $\hat{p} = p/2$. The G-S PPW is therefore equivalent to a non-physical nGS structure.

Yet, this dispersive equivalency gives insight about why G-S dispersion curves are more linear than the curves of the counterpart nGS waveguide with same period p. Fig. 5 displays the Brillouin diagram of the nGS waveguide with period p in blue (solid). At the right end of its first Brillouin zone, that is $\beta < \pi/p$, the dispersion curve bends, yielding an increased frequency dispersion. Indeed, a zero group velocity must be obtained when reaching the lower edge of the stopband between the first and second modes. The same bending occurs for the nGS waveguide with period $\hat{p} = p/2$, in purple in Fig. 5. However, because the period is halved, the first Brillouin zone is twice as large, and so this increased frequency dispersion appears at higher propagation constants. Finally, the G-S waveguide has the same dispersion curve (in red) as this equivalent nGS waveguide. But because it has a period p, its first mode corresponds to the linear part of the equivalent nGS curve, making it low-dispersive. This means that a G-S waveguide effectively behaves like a nGS waveguide with half the period in terms of dispersion.

https://doi.org/10.1017/S1759078723000090

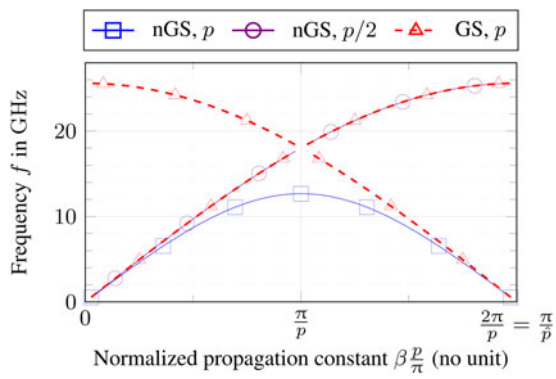

Fig. 5. Brillouin diagrams for the corrugated PPW shown in Fig. 4. The G-S waveguide (solid and dashed red curves) has dimensions $p = 4$ mm, $h = 1.5$ mm, $g = 0.2$ mm and $a = 1$ mm. It is compared to a nGS structure with the same dimensions (dashed blue curve), but also to its equivalent nGS structure (solid red curve), which has half the periodicity and twice the gap.

Linearization of the low-dispersive curves

In this section the dispersion equation (6) is linearized in G-S waveguides, assuming that the gap between the metasurfaces is small enough. This proves for the first time that the observed frequency dispersion is very weak. To this effect, the entries of the matrix $\underline{\boldsymbol{M}}$ are simplified, under the following assumptions:

(i) Subwavelength assumption: $p \leq \lambda/2$.
(ii) First Brillouin zone: $k \leq \beta \leq \pi/p$.
(iii) Small gap: $g \leq p/4$.
(iv) Shallow grooves: $h \leq p/8$.
(v) Thin corrugations : $a \leq \frac{p}{2}$.
(vi) Field variations on the corrugations are captured with one or two PPW modes.

Small grooves: one groove mode

When the width of the corrugations is very small compared to the wavelength, as is usually the case for metasurfaces, the field variability on the corrugated plate is small. Consequently, few modes are necessary to capture this variability. According to Fig. 2, for certain geometries it is even acceptable to keep only the TEM mode.

Assuming that only one mode ($M = 0$) in the corrugations is enough to yield a good approximate of the dispersion curve, the dispersion equation (6) is reduced to

$$M_{00} = 0, \tag{12}$$

where M_{00} is made of a sum of terms, each of which corresponds to one harmonic. According to (3) and the under assumption of small gap (8), M_{00} has the form

$$M_{00} = \gamma_0 + F_{00}^{(0)} + \sum_{s=-\infty s \text{ even},\ s\neq 0}^{+\infty} F_{00}^{(s)}, \tag{13}$$

where

$$F_{00}^{(s)} = -\frac{a^2 \coth\left(\frac{g}{2}\sqrt{\beta^{(s)2} - k_0^2}\right)}{\sqrt{\beta^{(s)2} - k_0^2}} \operatorname{sinc}^2\left(\beta^{(s)}\frac{a}{2}\right). \tag{14}$$

Assuming that the gap g is small enough, the fundamental harmonic term ($s = 0$) is dominant. Keeping only this term, and under the assumptions listed at the beginning of this section, M_{00} can be simplified in the first Brillouin zone as

$$M_{00} \simeq \frac{pa}{hk_0^2} - 2a^2 g k_0^2 \left[n_{\text{eff}}^2 - 1\right] = 0, \tag{15}$$

where $n_{\text{eff}} = \beta/k_0$ is the effective refractive index of a wave traveling along the z direction. This equation depends only on n_{eff}, and not on the frequency k_0, which can be factored out. This confirms that the corresponding dispersion curve is linear. The analytical solution of this equation is

$$n_{\text{eff}} = \sqrt{1 + \frac{2ha}{gp}}. \tag{16}$$

Although this solution is valid under strong geometrical assumptions, it is simple, and provides direct understanding about the influence of the various structure parameters on the refractive index. Moreover, it is only derivable if the contribution of the harmonic $s = -1$ can be dismissed, which is not true in the first Brillouin zone for the nGS structure. Therefore, the dispersion curve cannot be linearized, proving that the nGS waveguide is more dispersive than its G-S counterpart.

Medium grooves: two groove modes

The problem is extended to 2 modes in the corrugations. Consequently, the dispersion matrix $\underline{\boldsymbol{M}}$ becomes a 2×2 matrix, and is made of matrix coefficients M_{00}, M_{11}, and $M_{01} = -M_{10}$. For a small gap, thin and shallow corrugations, and in the entire first Brillouin zone, all these coefficients can be simplified. The simplified 2-mode dispersion equation is

$$\begin{aligned} M_{01}^2 + M_{00}M_{11} \simeq & \left\{\frac{\mathrm{j}4n_{\text{eff}}a^3}{g\pi^2\left[n_{\text{eff}}^2 - 1\right]}\right\}^2 \\ & + \left\{\frac{pa}{h} - \frac{2a^2}{g\left[n_{\text{eff}}^2 - 1\right]}\right\} \cdot \left\{-\frac{pa^2 \coth\left(\pi\frac{\mathrm{h}}{\mathrm{a}}\right)}{2\pi} - \frac{8a^4 n_{\text{eff}}^2}{g\pi^4\left[n_{\text{eff}}^2 - 1\right]}\right. \\ & \left. - \sum_{s=2s \text{ even}}^{+\infty} \frac{8\cos^2\left(s\pi\frac{a}{p}\right)\left(s\frac{2\pi}{p}\right)\coth\left[s\pi g\, p\right]}{\left[\left(s\frac{2\pi}{p}\right)^2 - \left(\frac{\pi}{a}\right)^2\right]^2}\right\} = 0. \end{aligned} \tag{17}$$

This equation depends only on the refractive index n_{eff} and not on the frequency k_0, proving that the G-S structure has a low-dispersive behavior in the first Brillouin zone and under the given structural assumptions. An analytical solution can be extracted from (17), that is

$$n_{\text{eff}} = \sqrt{gp + 2hagp + \frac{8}{\pi^4} pa^4 \frac{1}{u + v}}, \tag{18}$$

https://doi.org/10.1017/S1759078723000090

with

$$u = \frac{pa^2 \coth\left(\pi \frac{\mathrm{h}}{\mathrm{a}}\right)}{2\pi}, \tag{19}$$

$$v = \sum_{s=2s \text{ even}}^{+\infty} \frac{8\cos^2\left(s\pi\frac{a}{p}\right)\left(s\frac{2\pi}{p}\right)\coth[s\pi \mathrm{g}\,\mathrm{p}]}{\left[\left(s\frac{2\pi}{p}\right)^2 - \left(\frac{\pi}{a}\right)^2\right]^2}. \tag{20}$$

If all higher-harmonic contributions are neglected, as is done in (16), then (18) can be further simplified as

$$n_{\text{eff}} = \sqrt{1 + \frac{2ha}{gp}} \Bigg/ \sqrt{1 + \frac{16}{\pi^3}\frac{a^2}{gp\coth\left(\pi\frac{h}{a}\right)}}, \tag{21}$$

where the consideration of the second groove mode appears to apply a corrective term to (16).

The analytical solutions (18) and (21) are valid only for geometrically restricted G-S structures as described at the beginning of this section, with the additional assumption that the dispersion matrix must be truncated to two corrugation modes. Despite these limitations, it is interesting to remark that these formulas are valid over the whole Brillouin first zone i.e., for any $\beta < \pi/p$. For such structures, this proves that there is almost no dispersion over a wide band of frequencies. This result has been often observed in the literature and used to design low-dispersive metamaterials, but this is the first time that an effective index is obtained in a closed form not depending on the frequency under specific assumptions.

Importantly, the vanishing of the frequency dependence in (18) is due to the absence of the odd-order harmonics in the sum (20): the same approximations could not be done on the harmonic of order $s = -1$, where the frequency-dependence is non-negligible closer to the right edge of the Brillouin diagram.

Numerical results

In this Section we validate the two homogenized solutions (16) and (18) with independent results obtained with the eigensolver solver in the commercial software CST Microwave Studio.

Figs. 6 to 8 display the Brillouin diagrams of the G-S structure for various corrugation widths a. The true dispersion curve obtained with CST is compared to the dispersion curve computed with one or two modes and 50 harmonics in the complete MM equation (6). Moreover, the linearized dispersion curves obtained with (16) – 1 mode – and (18) – 2 modes – are also plotted, again with 50 harmonics.

Fig. 6a confirms that both linearizations (1 or 2 modes) are valid for thin corrugations, as the resulting dispersion curves fit the CST results. For larger values of a (e.g., $a = 1$ mm in Fig. 6b) the 1-mode curve is visibly different from the CST result, while the 2-mode curve is still very accurate. As can be expected, at low frequencies both linearized dispersion curves (dashed line) are always tangent to the corresponding exact curves (solid line), whatever the corrugation width.

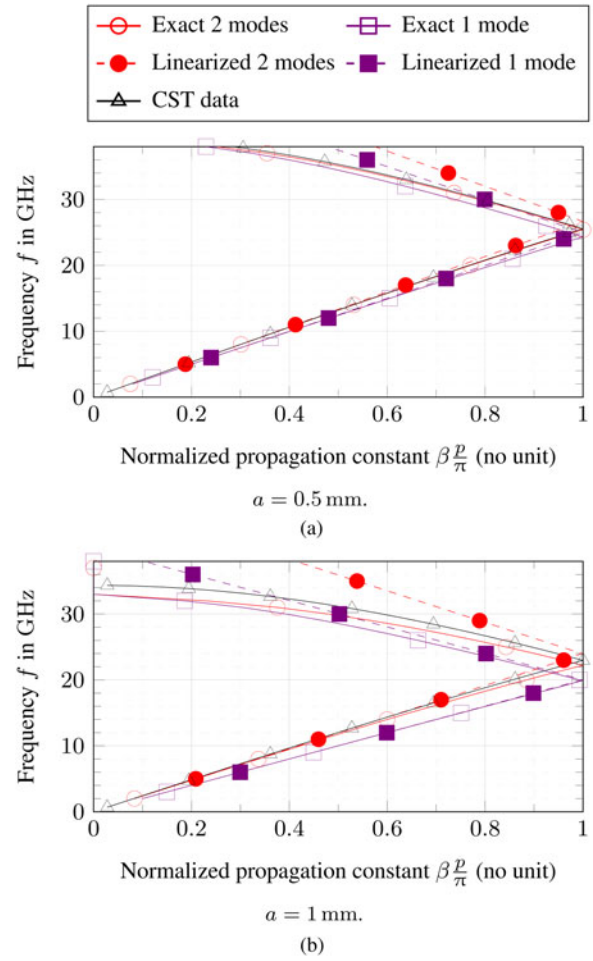

Fig. 6. Brillouin diagram for the G-S structure with $p = 4$ mm, $h = 0.5$ mm, $g = 0.1$ mm and varying corrugation width a. 50 harmonics are considered in all the homogenized models, (a) $a = 0.5$ mm, (b) $a = 1$ mm.

For larger sizes of the groove in Fig. 7, as expected, the accuracy is reduced also for the 2-mode approach, given that more modes are required to accurately describe the field variation at the surface of the grooves.

Nevertheless, Fig. 2 shows that for larger corrugations, fewer modes are required. That is why for large corrugations in Fig. 8, the 2-mode linearization approaches the CST curve again. However, it is to be noted that the non-linearized 2-mode curves are less accurate at the right-end of the Brillouin diagram. This is because larger corrugations lead to bigger approximations with increasing frequency, even if 2 modes are enough. The index formula (18) is thus valid in the first half of the Brillouin diagram, but less so with increasing frequency.

As long as the groove width is smaller than one third of the period, and provided that the hypotheses detailed in Section 'Linearization of the low-dispersive curves' are true, the 2-mode homogenization is very accurate in the entire first Brillouin zone, therefore over an ultra large band. This proves the extreme dispersionless feature of G-S corrugated structures over an ultra-wide band of frequencies when small gaps between the surfaces are considered. Further work on the computation of dispersionless closed-forms of the effective refractive index for larger grooves give very cumbersome results which will not be reported here.

https://doi.org/10.1017/S1759078723000090

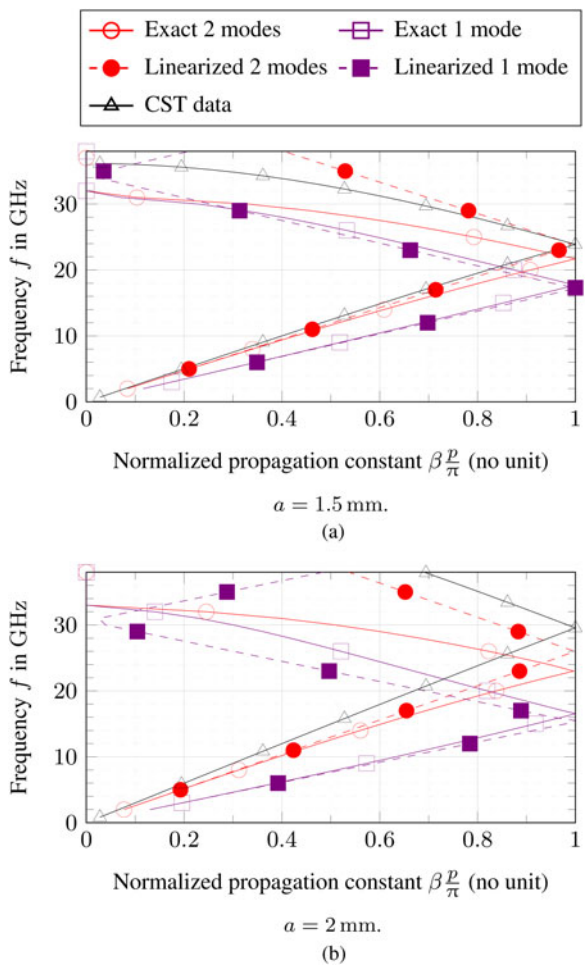

Fig. 7. Brillouin diagram for the G-S structure with $p = 4$ mm, $h = 0.5$ mm, $g = 0.1$ mm and varying corrugation width a. 50 harmonics are considered in all the homogenized models, (a) $a = 1.5$ mm. (b) $a = 2$ mm.

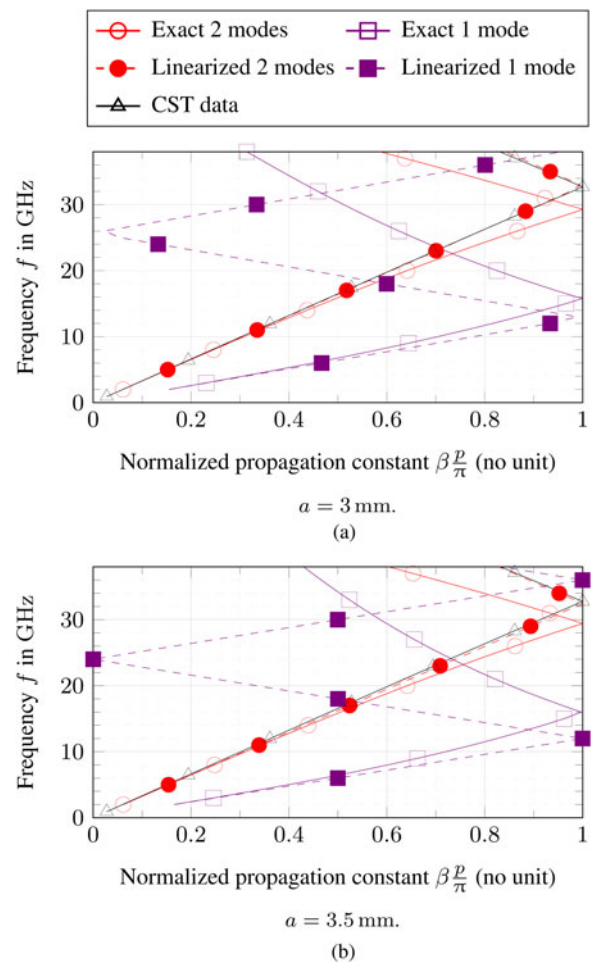

Fig. 8. Brillouin diagram for the G-S structure with $p = 4$ mm, $h = 0.5$ mm, $g = 0.1$ mm and varying corrugation width a. 50 harmonics are considered in all the homogenized models, (a) $a = 3$ mm. (b) $a = 3.5$ mm.

Conclusion

The MM method gives analytical access to the impact of the different Floquet harmonics on the behavior of corrugated metasurface waveguides. The dispersive differences between G-S and nGS waveguides, notable when the gap between the metasurfaces is small, are the consequence of the a reduced number of dominant harmonics. A similar result can be obtained for two-dimensional metasurfaces when using the extended MM developed in [30].

Keeping only half the number of harmonics in the G-S dispersion equation also explains the low-dispersive behavior by identifying an equivalent nGS waveguide with half the period. It must be kept in mind that this equivalency only concerns the dispersive behavior of such a structure. Moreover, the existence of an equivalent nGS waveguide should be understood under the necessary hypotheses: not only is this equivalency valid only for the particular case of the corrugated PPW with small gaps, but also the equivalent nGS waveguide may not be physical. When it is, from a practical point of view, the GS waveguide needs only half the number of corrugations for a given length, which is a considerable manufacturing gain.

As a consequence of the dismissible harmonics, the low-dispersive behavior of GS is proven in this paper for shallow corrugations, for which it appears that there is a singularity in the simplified dispersion equation that moves linearly with increasing frequency. This results in closed-form expressions for the effective refractive index of G-S waveguides, that are frequency-independent and valid in the entire first Brillouin zone. This shows the absence of frequency dispersion over an ultra-wide bandwidth of frequencies. For fast modeling of G-S corrugated waveguides without geometry restrictions, one can turn to the accurate quasi-static formula derived in [23], that take the low-dispersive behavior proven in this paper as a pre-requisite, or to the formula for holey two-dimensional structures in [31].

Acknowledgements. This work was supported by the French government under the ANR grant HOLeYMETA ANR JCJC 2016 ANR-16-CE24-0030.

Conflict of interest. The author(s) declare none.

References

1. **Y Wang, J Li, L Huang, Y Jing, A Georgakopoulos and P Demestichas** (2014) 5G mobile: spectrum broadening to higher-frequency bands to support high data rates. *IEEE Vehicular Technology Magazine* **9**, 39–46.
2. **CL Holloway, EF Kuester, JA Gordon, J O'Hara, J Booth and DR Smith** (2012) An overview of the theory and applications of metasurfaces: the two-dimensional equivalents of metamaterials. *IEEE Antennas and Propagation Magazine* **54**, 10–35.

https://doi.org/10.1017/S1759078723000090

3. **O Quevedo-Teruel, H Chen, A Diaz-Rubio, G Gok, A Grbic, G Minatti, E Martini, S Maci, GV Eleftheriades, M Chen, NI Zheludev, N Papasimakis, S Choudhury, ZA Kudyshev, S Saha, H Reddy, A Boltasseva, VM Shalaev, AV Kildishev, D Sievenpiper, C Caloz, A Alu, Q He, L Zhou, G Valerio, E Rajo-Iglesias, Z Sipus, F Mesa, R Rodriguez-Berral, F Medina, V Asadchy, S Tretyakov and C Craeye** (2019) Roadmap on metasurfaces. *Journal of Optics* **21**, 073002.
4. **DM Pozar** (2011) *Microwave Engineering*, 4th ed. Hoboken, NJ: John Wiley & Sons.
5. **O Quevedo-Teruel, M Ebrahimpouri and F Ghasemifard** (2018) Lens antennas for 5 g communications systems. *IEEE Communications Magazine* **56**, 36–41.
6. **O Quevedo-Teruel, G Valerio, Z Sipus and E Rajo-Iglesias** (2020) Periodic structures with higher symmetries: their applications in electromagnetic devices. *IEEE Microwave Magazine* **21**, 36–49.
7. **O Quevedo-Teruel, Q Chen, F Mesa, NJG Fonseca and G Valerio** (2020) On the benefits of glide symmetries for microwave devices. *IEEE Journal of Microwaves* **1**, 457–469.
8. **O Quevedo-Teruel, M Ebrahimpouri and MNM Kehn** (2016) Ultrawideband metasurface lenses based on off-shifted opposite layers. *IEEE Antennas and Wireless Propagation Letters* **15**, 484–487.
9. **M Ebrahimpouri, A Algaba Brazalez, L Manholm and O Quevedo-Teruel** (2018) Using glide-symmetric holes to reduce leakage between waveguide flanges. *IEEE Microwave and Wireless Components Letters* **28**, 473–475.
10. **O Dahlberg, RC Mitchell-Thomas and O Quevedo-Teruel** (2017) Reducing the dispersion of periodic structures with twist and polar glide symmetries. *Scientific Reports* **7**, 1.
11. **A Alex-Amor, F Ghasemifard, G Valerio, M Ebrahimpouri, P Padilla, JMF Gonzalez and O Quevedo-Teruel** (2020) Glide-symmetric metallic structures with elliptical holes for lens compression. *IEEE Transactions on Microwave Theory and Techniques* **68**, 4236–4248.
12. **M Ebrahimpouri, E Rajo-Iglesias, Z Sipus and O Quevedo-Teruel** (2018) Cost-effective gap waveguide technology based on glide-symmetric holey EBG structures. *IEEE Transactions on Microwave Theory and Techniques* **66**, 927–934.
13. **Q Chen, F Ghasemifard, G Valerio and O Quevedo-Teruel** (2018) Modeling and dispersion analysis of coaxial lines with higher symmetries. *IEEE Transactions on Microwave Theory and Techniques* **66**, 4338–4345.
14. **E Rajo-Iglesias, M Ebrahimpouri and O Quevedo-Teruel** (2018) Wideband phase shifter in groove gap waveguide technology implemented with glide-symmetric holey EBG. *IEEE Microwave and Wireless Components Letters* **28**, 476–478.
15. **M Bagheriasl, J Sarrazin and G Valerio, Reconfigurable waveguides using glide-symmetric bed of nails: design of an all-metal switch at millimetre-wave band, arXiv:2007.08021 [eess], Jul. 2020, Accessed: 21, 2020. [Online]. Available: http://arxiv.org/abs/2007.08021.**
16. **D Cavallo and C Felita** (2017) Analytical formulas for artificial dielectrics with nonaligned layers. *IEEE Transactions on Antennas and Propagation* **65**, 5303–5311.
17. **G Valerio, DR Jackson and A Galli** (2010) Formulas for the number of surface waves on layered structures. *IEEE Transactions on Microwave Theory and Techniques* **58**, 1786–1795.
18. **Z Sipus, H Merkel and P- Kildal** (1997) Green's functions for planar soft and hard surfaces derived by asymptotic boundary conditions. *Antennas and Propagation IEE Proceedings - Microwaves* **144**, 321–328.
19. **M Bosiljevac, Z Sipus and P-S Kildal** (2010) Construction of Green's functions of parallel plates with periodic texture with application to gap waveguides – a plane-wave spectral-domain approach. *IET Microwaves, Antennas & Propagation* **4**, 1799–1810.
20. **M Bagheriasl, O Quevedo-Teruel and G Valerio** (2019) Bloch analysis of artificial lines and surfaces exhibiting glide symmetry. *IEEE Transactions on Microwave Theory and Techniques* **67**, 2618–2628.
21. **F Ghasemifard, M Ebrahimpouri, M Norgren and O Quevedo-Teruel** (2017) Mode matching analysis of two dimensional glide-symmetric corrugated metasurfaces, in *2017 11th European Conference on Antennas and Propagation (EUCAP)*, pp. 749–751.
22. **F Ghasemifard, M Norgren and O Quevedo-Teruel** (2018) Dispersion analysis of 2-d glide-symmetric corrugated metasurfaces using mode-matching technique. *IEEE Microwave and Wireless Components Letters* **28**, 1–3.
23. **B Fischer and G Valerio** (2021) Ultra-wideband homogenization of a glide-symmetric parallel-plate waveguide, in *2021 15th European Conference on Antennas and Propagation (EuCAP), Düsseldorf*, pp. 1–4.
24. **B Fischer and G Valerio** (2022) Homogenization and Dispersion Properties of Glide-Symmetric Corrugated Metasurfaces, in *2022 Microwave Mediterranean Symposium (MMS)*, Pizzo Calabro, pp. 1–5.
25. **G Valerio, F Ghasemifard, Z Sipus and O Quevedo-Teruel** (2018) Glide-symmetric all-metal holey metasurfaces for low-dispersive artificial materials: modeling and properties. *IEEE Transactions on Microwave Theory and Techniques* **66**, 3210–3223.
26. **PJ Crepeau and PR McIsaac** (1964) Consequences of symmetry in periodic structures. *Proceedings of the IEEE* **52**, 33–43.
27. **R Mittra and S Laxpati** (1965) Propagation in a wave guide with glide reflection symmetry. *Canadian Journal of Physics*. **43**, 353–372.
28. **A Hessel, MH Chen, RCM Li and AA Oliner** (1973) Propagation in periodically loaded waveguides with higher symmetries. *Proceedings of the IEEE* **61**, 183–195.
29. **B Fischer and G Valerio** (2021) Broadband dispersionless glide-symmetric parallel-plate waveguide with small corrugations, in *2021 15th European Conference on Antennas and Propagation (EuCAP)*, Düsseldorf, pp. 1–4.
30. **F Ghasemifard, M Norgren, O Quevedo-Teruel and G Valerio** (2018) Analyzing glide-symmetric holey metasurfaces using a generalized floquet theorem. *IEEE Access* **6**, 71743–71750.
31. **B Fischer and G Valerio** (2022) Quasi-static homogenization of glide-symmetric holey parallel-plate waveguides with ultra-wideband validity. *IEEE Transactions on Antennas and Propagation* **70**, 10569–10582.

Boris Fischer received the M.Sc. degree with high distinction in electrical engineering and information technology in 2019 at the Technische Universität München, Munich, Germany, and the Ph.D. degree in electromagnetics in 2022 at the Laboratoire Génie Electrique et Electronique de Paris, Sorbonne Université, Paris, France. His current research is focused on wave propagation in periodic structures at millimeter waves and dispersion of higher-symmetric waveguides made of metallic metasurfaces. In 2022, Dr. Fischer was a co-author of the paper awarded with the Best Student Paper Award at the 16th European Conference on Antennas and Propagation, Madrid, Spain, and he was a finalist for the Best Electromagnetics Paper at the same conference.

Guido Valerio received the Ph.D. degree in electromagnetics in 2009 from La Sapienza University, Rome, Italy. In 2008 he was a Visiting Scholar at the University of Houston, TX, USA. From 2011 to 2014, he was a researcher at IETR, France. Since 2014 he is at Sorbonne Université, Paris, France, where is a Professor. His scientific interests involve antenna design and numerical methods for wave propagation and scattering, modal properties of multilayered structures, full-wave methods for SIW, modeling and design of periodic structures. Dr. Valerio serves as Associate Editor for the IEEE Transactions on Antennas and Propagation and the IEEE Access journals, and is the Main Chair of the SyMat COST Action. In 2014, of the RMTG Award for junior researchers at the IEEE APS Symposium. In 2018, 2020, and 2022, he was a co-author of the best papers in different categories at the European Conference on Antennas and Propagation.

https://doi.org/10.1017/S1759078723000090